View metadata, citation and similar papers at core.ac.uk
brought to you by CORE
provided by Digital.CSIC

PHYSICAL REVIEW B **85**, 134437 (2012)

Determination of the magnetostrictive atomic environments in FeCoB alloys

J. Díaz,* C. Quirós, and L. M. Alvarez-Prado
Departamento de Física, Facultad de Ciencias, Universidad de Oviedo-CINN, Avenida de Calvo Sotelo s/n, Oviedo-33007, Spain and Centro de Investigación en Nanomateriales y Nanotecnología (CINN), CSIC-Universidad de Oviedo-Principado de Asturias, 33428 Llanera, Spain

C. Aroca
E.T.S.Ing. Telecomunicación, Ciudad Universitaria s/n Madrid, 28040 Madrid, Spain

R. Ranchal
Departamento de Física de Materiales, Universidad Complutense de Madrid. Madrid 28040, Spain

M. Ruffoni and S. Pascarelli
European Synchrotron Radiation Facility, 6 Rue Jules Horowitz, BP220, F-38043 Grenoble Cedex, France
(Received 24 October 2011; revised manuscript received 6 February 2012; published 23 April 2012)

The atomic environments of Fe and Co involved in the magnetostriction effect in FeCoB alloys have been identified by differential extended x-ray fine structure (DiffEXAFS) spectroscopy. The study, done in amorphous and polycrystalline FeCoB films, demonstrates that the alloys are heterogeneous and that boron plays a crucial role in the origin of their magnetostrictive properties. The analysis of DiffEXAFS in the polycrystalline and amorphous alloys indicates that boron activates magnetostriction when entering as an impurity into octahedral interstitial sites of the Fe bcc lattice, causing its tetragonal distortion. Magnetostriction would be explained then by the relative change in volume when the tetragonal axis of the site is reoriented under an externally applied magnetic field. The experiment demonstrates the extreme sensitivity of DiffEXAFS to characterize magnetostrictive environments that are undetectable in their related EXAFS spectra.

DOI: 10.1103/PhysRevB.85.134437 PACS number(s): 61.05.cj, 61.43.Dq, 75.80.+q, 75.50.Kj

I. INTRODUCTION

One of the main difficulties to unveil the exact mechanism of the magnetic anisotropy and magnetostriction in amorphous alloys is the intrinsic uncertainty in the description of the atomic environments of their ferromagnetic atoms. Unlike in a crystal, where the atomic environments are reduced to those in the unit cell, the number of possible arrangements between atoms in an amorphous alloy is huge and undefined.[1,2] It is technically impossible to distinguish between all the different atomic environments in an amorphous material, having only information of the average atomic distribution. In fact, it is usually assumed that the amorphous materials are homogeneous. But the presence of magnetostriction and magnetic anisotropy in amorphous alloys is, in principle, noncompatible with a disordered and homogeneous structure.[3] The origin of these properties is usually associated with local perturbations in the atomic environments breaking such assumed homogeneity. The question to address is to know if such a local perturbation occurs with higher or lower intensity in all the atomic environments of the amorphous alloy, or it happens only at specific atomic sites and, if that is the case, how to identify them. The microscopic theories that try to understand the magnetostriction in amorphous matter are mostly phenomenological and they are based on the so-called standard model of magnetostriction of Callen and Callen.[4] This model differentiates between single-ion and double-ion interactions. In the single-ion interaction, magnetostriction and/or magnetic anisotropy should arise from crystal field effects at the specific atomic environment, whereas the double-ion interaction considers anisotropic interatomic interactions. Single-ion interaction explains quite well the magnetostriction in transition metal/rare earths. In this case, the coupling of the magnetic moment of the rare earth with the crystal field is intuitively understood given its strong spin-orbit interaction, which causes the mentioned properties. The magnetostrictive properties of amorphous transition metal/metalloid (TM-M) alloys like FeCoB and FeB are also believed to be caused by this single-ion interaction, attending to indirect experimental proofs based on the analysis of the temperature dependence of their magnetostriction coefficient.[5] However, the orbital moment in transition metals is strongly quenched in a solid. Therefore the metalloid should interact with the ferromagnetic transition metal in similar way as the rare earth, i.e., increasing the spin-orbit interaction at the specific site.

FeCoB alloys reach their highest magnetostrictive strain in Fe-rich compositions and at 20% atomic boron concentrations. This boron concetration corresponds to the eutectic concentration for FeB and CoB alloys.[5] In FeB, this is the concentration that favors the highest magnetostricive strain, of the order of 30 ppm, similar to values found in FeCoB. On the other hand, the magnetostrictive strain in CoB is negative with magnetostriction coefficients not higher than $|-10|$ ppm.[6,7] FeCo has a relatively large and anisotropic magnetostrictive strain in its crystalline state ($\lambda_{111} = 60$ ppm and $\lambda_{100} = 210$ ppm),[8] but its magnetostriction will probably vanish if long-range order is broken as in a disordered or amorphous solid.[9] Therefore out of the three different potentially magnetostrictive environments in amorphous FeCoB, i.e., FeCo, FeB, and CoB, FeB is presumably the environment that would give rise to the magnetostrictive properties of glassy FeCoB.

 ©2012 American Physical Society

Boron belongs to the same column (IIIa) of the periodic table as Ga and Al. The alloys of Fe with either of these two other metalloids at their eutectic concentration strongly enhance the magnetostrictive strain in Fe.[10] The origin of the magnetostriction in these alloys is still discussed. Some theoretical and experimental works support the extrinsic origin of their magnetostrictive properties, based on the reorientation of tetragonal defects resulting from the process of transformation of the structure of the alloy from bcc to fcc such as with increasing metalloid concentration structures.[11–13] This model assumes that the alloy is heterogeneous, as experimentally recognized by electron microscopy[14] and neutron scattering.[15] On the other side, there are the rigid band models that consider that the magnetostriction of these alloys is intrinsic and derives from the specific electronic structure of the crystal. The magnetostriction in these models is driven by critical changes in the spin orbit interaction due to a strain induced modification of magnetocrystalline anisotropy.[16] This theory predicts a higher enhancement of the magnetostriction at the sites near the metalloid, as observed experimentally by differential extended x-ray fine structure (DiffEXAFS) in FeGa.[17] Additional experiments to test this prediction, aimed at observing changes in magnetostriction based on electron occupancy were, however, not successful.[18]

Heterogeneities have also been observed in FeB at concentrations just below the eutectic point.[19] Although they were not fully identified, they were associated with the highly metastable orthorhombic Fe_3B phase, of similar structure as cementite, which has reported Invar properties.[20,21] Magnetostriction in FeB has been attributed to this phase although with no conclusive proofs. Like in FeGa, the phase diagram of FeB at boron concentrations near the eutectic point is highly metastable showing a transformation from the bcc Fe lattice to an fcc-like structure as boron concentration is increased.[22,23] Once in the glassy state, those heterogeneities are not observed by high-resolution electron microscopy. However, its recrystallization produces the formation of bcc Fe precipitates with boron occupying both substitutional and interstitial sites. Only the crystallites with interstitial boron were coarsening resistant never reaching sizes larger than 40 nm.[24] When boron enters as an interstitial in bcc Fe, it expands the volume of the cell and distorts it tetragonally. It is known that other interstitial impurities of similar atomic radius than boron, like carbon and nitrogen, when entering the bcc Fe lattice cause an enhancement of the magnetic moment and anisotropy of the surrounding Fe atoms.[24–28] Actually, the enhancement of the magnetic anisotropy observed in FeB alloys has in some cases been explained assuming such a tetragonal distortion of the bcc Fe lattice by interstitial boron.[29]

All this discussion conveys that a fundamental step for the understanding of the magnetostriction in these alloys is the identification of the atomic environments that generate it. DiffEXAFS is a recently developed technique, extraordinarily powerful for the study of magnetostriction in solids, which is able to measure atom displacements down to the femtometer scale[8] in single crystals,[30] polycrystals,[17] and amorphous matter.[31] Its characteristics make it ideal for the study of magnetostriction at the atomic level in disordered, heterogeneous, and/or amorphous alloys like FeCoB: it is a local probe, chemically and elemental sensitive, and highly selective, giving structural information from only those atomic environments that change their strain under a magnetic field.

In the present work, FeCoB alloys with different concentrations are prepared to yield both polycrystalline and amorhous samples. The atomic environments of all samples are investigated by EXAFS and DiffEXAFS. EXAFS analysis of the polycrystalline samples reveals a local structure that can be described as a mixture of bcc and fcc phases. When passing from the crystalline to the amorphous state with increasing boron, only an fcc-like local structure is retained, confirming previous observations[22] on similar alloys. This is a common behavior in Invar and magnetostrictive alloys,[32] FeCo included and might indicate that such a transformation originates an intermediate metastable phase with magnetostrictive properties.

The environments probed by DiffEXAFS strongly differ from those detected by EXAFS, demonstrating that the magnetostriction is localized only at certain atomic environments. Therefore these alloys are found to be heterogenous, with the presence of at least two coexisting phases of different local structure, one magnetostrictive and one not magnetostrictive.

The environments identified by DiffEXAFS in the polycrystalline alloy correspond to a tetragonally distorted bcc Fe lattice whose distortion is likely caused by interstitial boron, thereby discarding the orthorhombic Fe_3B phase as the possible cause of magnetostriction in these alloys. Interestingly, the magnetostrictive environment found in the polycrystalline alloy is preserved in the amorphous state to first neighbors. DiffEXAFS also confirms that the possible contribution to magnetostrive strain by FeCo environments is negligible.

The paper is organized as follows. The next section (Sec. II) describes the experimental aspects, including sample preparation and EXAFS and DiffEXAFS measurements. Section III presents the results of an independent analysis of the EXAFS (IIIa) and DiffEXAFS (IIIb) of all samples. The former provides average local structural parameter values, whereas the latter provides the structural parameters relative to the magnetostrictive environments only. In Sec. IV, we use this information to extract, from the EXAFS spectra, the relative proportion of the magnetostrictive and nonmagnetostrictive phase in each sample. This procedure allows one to (i) obtain quantitative values for the microscopic (atomic level) magnetostriction coefficients and (ii) extract the structural parameters of the nonmagnetostrictive environments. This method works well for the amorphous samples, characterized by higher proportion of magnetostrictive environments. For the polycrystalline samples, we were not able to obtain a reliable estimate for the proportion of magnetostrictive to nonmagnetostrictive environments, so we use an alternative method (described in Sec. IV) that allows one to extract the macroscopic (averaged over the whole sample) magnetostriction coefficients only. Finally, in Sec. V, we discuss the results obtained and suggest a model to explain the magnetostrictive properties of these alloys.

II. EXPERIMENT

The alloys were deposited in the form of thin films on glass substrates by magnetron sputtering using a single target. The targets were prepared by mixing high-purity iron, cobalt, and boron powders with the desired composition. This powder

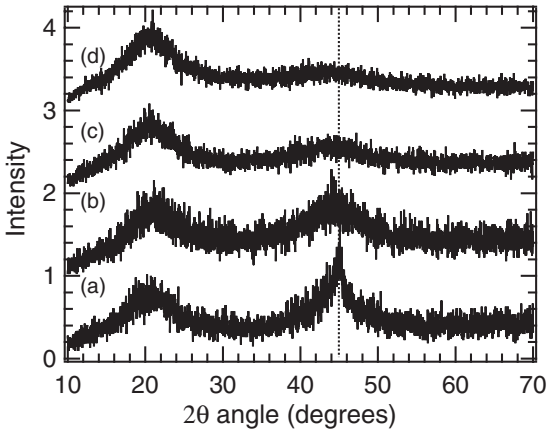

FIG. 1. θ-2θ scans of the FeCoB analyzed alloys: (a) $(Fe_{80}Co_{20})_{90}B_{10}$, (b) $(Fe_{80}Co_{20})_{80}B_{20}$, (c) $(Fe_{50}Co_{50})_{80}B_{20}$, and (d) $(Fe_{10}Co_{90})_{80}B_{20}$. The diffracted intensity of the 6-μm thick films was normalized to the intensity of the broad peak centered at $2\theta \approx 21^\circ$ related to the diffracted intensity from the substrate. A constant was added to the scans for a better view.

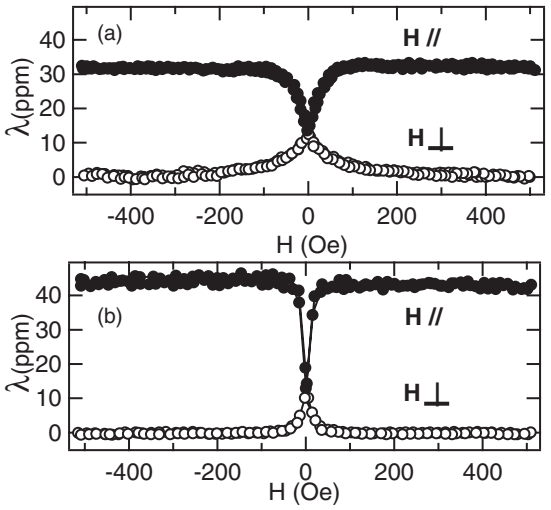

FIG. 2. Magnetostrictive measurements of (a) $(Fe_{80}Co_{20})_{80}B_{10}$ and (b) $(Fe_{80}Co_{20})_{80}B_{20}$ alloys deposited onto a cantilever beam when the field was applied parallel (solid spots, λ_L) and perpendicular (empty spots, λ_T) to the cantilever beam.

was compacted under high pressure in an Ar atmosphere. The base pressure of the deposition vacuum chamber was below 10^{-7} mbar. Ar pressure during sputtering was 5×10^{-3} mbar. The deposition rate was of 46 nm/min. The thickness of the films was 6 μm. At such a thickness, the films were easily peeled off the substrate. These self-sustained films were fixed to the sample holders using vacuum grease. This avoided the use of an excessive pressure to set the samples in place, which might have interfered in the measurement of their magnetostriction. The alloy concentrations were chosen in order to compare polycrystalline with amorphous states with the highest magnetostriction coefficient ($Fe_{80}Co_{20}$). The boron concentration was 10% at. and 20% at. (eutectic concentration), respectively, in the polycrystalline and amorphous states. To understand the role of Co, two other amorphous alloys were prepared with increased Co concentration keeping the boron atomic concentration at the eutectic point (20% at.): $(Fe_{50}Co_{50})_{80}B_{20}$ and $(Fe_{10}Co_{90})_{80}B_{20}$.

Figure 1 shows the diffraction pattern of the analyzed alloys, which consisted in two broad peaks. The first peak centered at $2\theta \approx 20^\circ$ is scattering from the (amorphous) polimeric substrate. The intensity of the patterns was normalized to the intensity of this peak. The second peak centered at about $2\theta = 45^\circ$ decreases in intensity with Co content. A low-intensity sharp peak can be distinguished only in the alloy with the lowest boron content. The alloy of similar Fe and Co concentration but higher boron content seems to have its highest intensity $\approx1^\circ$ downshifted. The point of highest intensity is more difficult to define in the other two alloys. The patterns of all the alloys are typical of amorphous alloys with possible traces of polycristalline regions.[33,34] The presence of polycrystalline environments is evident in the alloy with the lowest boron content, and it is possible in the alloy with the same concentration of Fe but 20% of boron. The EXAFS analysis, presented in Sec. III A of this work, will go deeper in the detailed atomic environments in all of the alloys.

The macroscopic magnetostriction coefficients (λ_M) of alloys of similar concentration than those analyzed were obtained by measuring the difference in the bending of a cantilever beam (covered with a thin film of the alloy to be measured) when the field was applied parallel and perpendicular to its longitudinal direction.[35,36] The measured values were in close agreement with those reported in the literature.[5,33,37] Figure 2 shows the magnetostrictive response of the alloys with concentrations $(Fe_{80}Co_{20})_{80}B_{10}$ and $(Fe_{80}Co_{20})_{80}B_{20}$. Their macroscopic magnetostriction coefficients, 20($\pm$5) and 30($\pm$5) ppm, respectively, can be deduced from the figure, where $\lambda_M = 2/3(\lambda_L - \lambda_T)$. The polycristalline alloy $[(Fe_{80}Co_{20})_{80}B_{10}]$ was magnetically harder than the alloy with higher boron concentration, as it can be appreciated in Fig. 2, attending to the magnetic fields needed to reach their saturation magnetostriction values. The amorphous alloy rich in Co $[(Fe_{10}Co_{90})_{80}B_{20}]$ did not present a significant macroscopic magnetostriction, as expected.[5]

The DiffEXAFS experiment was carried out using the energy dispersive XAS spectrometer of the European Synchrotron Radiation Facility (ESRF), on ID24.[38] The highest scattering wave number reached in the DiffEXAFS and EXAFS spectra was 9.5 Å^{-1}. High-purity polycrystalline cobalt and iron foils were measured as a reference for the calculation of the passive electron reduction factor S_0^2. It was 0.75 for the Fe K edge and 0.9 for the Co K edge. The set up for DiffEXAFS was similar to that reported in previous experiments.[8,17] The spectra were measured in transmission. A DiffEXAFS spectrum is obtained from the difference between two spectra, one acquired with a magnetic field applied parallel to the polarization vector and a second obtained with the magnetic field rotated 90° and transversal to the beam. The amplitude of DiffEXAFS is highly reduced with respect to the corresponding EXAFS amplitude of an order of magnitude proportional to the magnetostriction coefficient, which was especially small in the samples measured in this experiment ($\approx$30 ppm). This number is not far from the detection limit of the technique estimated in 5 ppm and, therefore, the signal to noise ratio was extremely small. This was improved by

averaging the spectra over few thousands of EXAFS pairs. The acquisition time for each EXAFS pair was of about 2 s.

The background of the EXAFS and DiffEXAFS spectra was removed using the routine AUTOBACK in the application IFEFFIT.[39] All the spectra were fitted in the k range available, from 2.9 to 9.5 $Å^{-1}$ for the EXAFS spectra, and from 2.5 to 9.5 $Å^{-1}$ for the DiffEXAFS spectra, without performing any previous Fourier transform filtering. All the spectra presented in R space in this work was Fourier transformed from the portion of the spectra used for their fit, using the corresponding routine in IFEFFIT.

III. RESULTS

In this section, we present separately the EXAFS and DiffEXAFS analysis for all samples. The EXAFS analysis (see Sec. III A) is based on testing possible models for the local structure using a least squares fitting procedure, with free parameters the interatomic distance (R) and the mean-square relative displacement (σ^2) for each coordination shell. Constraints in coordination numbers are imposed between different coordination shells of a particular crystallographic structure. A similar approach is used to analyze the DiffEXAFS (see Sec. III B), except that here no coordination number constraint is imposed between different coordination shells, because the amplitude of each path is determined by the magnetostrictive strain on the associated bonds, which is unknown.

A. EXAFS spectra

Figure 3 compares the XAS spectra of polycrystalline bcc Fe with polycrystalline $(Fe_{80}Co_{20})_{90}B_{10}$ and amorphous $(Fe_{80}Co_{20})_{80}B_{20}$ alloys. Figure 4 shows the EXAFS spectra of all the alloys obtained at the Fe K edge represented in k space after background substraction. The spectra of the alloys in the Co K edge were very similar, differing only in amplitude due to the larger electron passive factor S_0^2 at Co, and only one of the

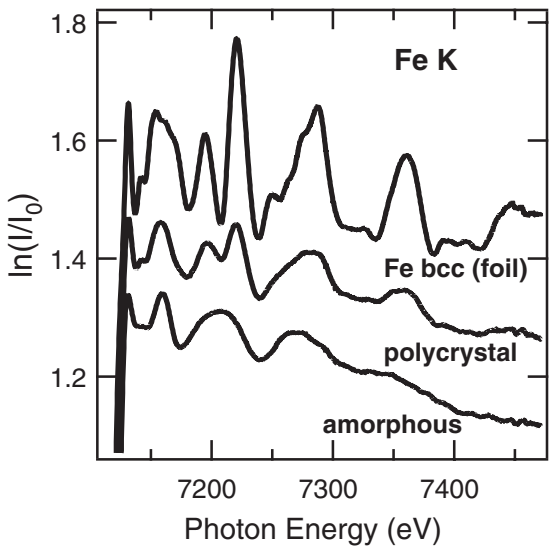

FIG. 3. Normalized XAS spectrum of an Fe foil used as reference, compared to the normalized spectra of $(Fe_{80}Co_{20})_{90}B_{10}$ (polycrystalline) and $(Fe_{80}Co_{20})_{80}B_{20}$ (amorphous). All the spectra were obtained with the dispersive spectrometer.

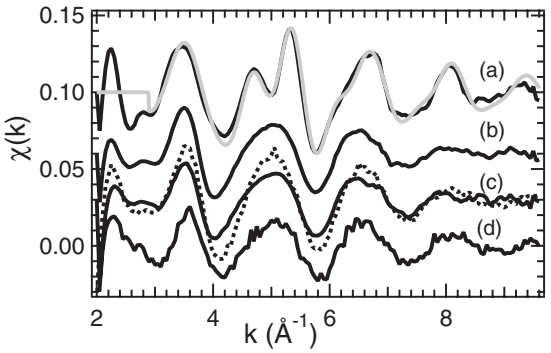

FIG. 4. Normalized EXAFS spectra obtained at the Fe K edge of (a) $(Fe_{80}Co_{20})_{90}B_{10}$, (b) $(Fe_{80}Co_{20})_{80}B_{20}$, (c) $(Fe_{50}Co_{50})_{80}B_{20}$, and (d) $(Fe_{10}Co_{90})_{80}B_{20}$ represented in k space. The grey line on the spectrum (a) is the fit to the spectrum of the polycrystalline alloy using the parameters of Table I. The dashed spectrum overlapped in (c) was obtained at the Co K edge.

spectra was displayed. The amplitude of the spectra decreased with boron concentration due to the increasing amorphization of the film caused by the metalloid.[40] The changes in the spectra were better noticed in their Fourier transformed form (R space)(see Fig. 5). The $\chi(R)$ spectrum of the polycrystalline alloy was similar to that of a bcc Fe lattice but with several significant differences. The main peak at low R (2 Å), which represents scattering from first neighbors, was more intense than the rest of the spectra when compared to the spectrum of bcc Fe, indicating a higher disorder for second neighbors shells in the polycrystalline alloy. Also, the shoulder at about 2.7 Å was better resolved than the same feature in bcc Fe. Finally, the region between 3 and 4 Å of the alloy spectrum did not match that of bcc Fe. The intensity at this region peaks near 3 Å, whereas in bcc Fe it peaks at 3.7 Å. The intensity of the spectrum of the amorphous alloy was significantly reduced compared to that of the polycrystal. The intensity due to scattering from second neighbors was also much smaller although more intense than what would be expected

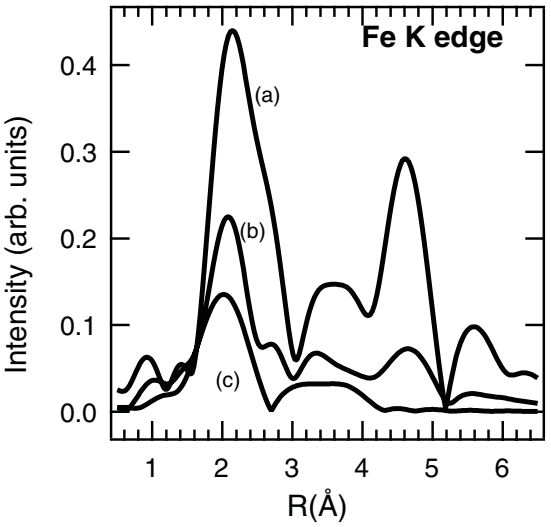

FIG. 5. Fourier transform of the normalized EXAFS spectra of (a) the Fe foil used as reference, (b) the polycrystalline alloy $(Fe_{80}Co_{20})_{90}B_{10}$, and (c) the amorphous alloy $(Fe_{80}Co_{20})_{80}B_{20}$.

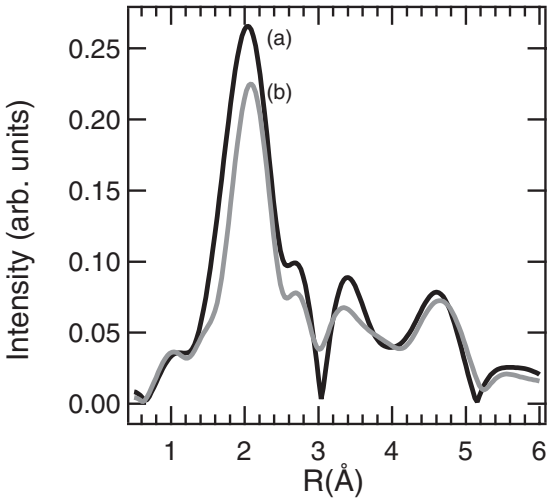

FIG. 6. Fourier transform of the normalized EXAFS spectra of the polycrystalline alloy $(Fe_{80}Co_{20})_{90}B_{10}$ at the (a) Co K edge (black line) and (b) Fe K edge (grey line).

in an ideal amorphous material, where it usually vanishes.[41,42] The spectra of the alloys at the Co edge were very similar in shape to those obtained at the Fe K edge. Figure 6 compares the EXAFS spectra of the polycrystalline alloy obtained at the Co and Fe K edges. The difference in intensity is caused by the higher electron passive factor S_0^2 at Co. The Fe K edge spectrum is shifted to higher bond lengths, as also occurs for the amorphous alloys.

The analysis of the EXAFS spectra was done using the known EXAFS expression for $k\chi(k)$:[43]

$$k\chi(k) = \sum_i \frac{N_i S_0^2 f_i(k)}{R_i^2} e^{-2\sigma_i^2 k^2} e^{-2R_i/\lambda(k)} \sin[2kR_i + \phi_i(k)]. \quad (1)$$

N_i is the number of atoms of i type around the absorbing atom, $f_i(k)$ is the backscattering amplitude function of atoms of type i around the absorbing species, R_i is the distance between the absorbing atom and the atom of type i, $e^{-2\sigma_i^2 k^2}$ is the Debye-Waller factor, $e^{-2R_i/\lambda(k)}$ is a mean-free path term that takes into account the inelastic losses, and $\phi_i(k)$ is the total phase shift in the electron scattering. The functions $f_i(k)$, $e^{-2R_i/\lambda(k)}$, and the total phase shift $\phi_i(k)$ were calculated using the FEFF8.10 code.[44] The parameters to fit for each shell i were the number of atoms N_i, the distance R_i, and the thermal and intrinsic disorder in the shell represented in the Debye-Waller factor by σ_i. The parameter S_0^2 was used to correct for losses due to multielectron excitations that are not accounted for in the elastic scattering model used to fit the spectra.[43] This parameter was obtained from the EXAFS spectra of polycrystalline Co and Fe foils.

The range of spectrum fitted covered the contribution from distant neighbors (shells) with large enough intensity to be considered. This range extended up to about 6 Å in the spectrum of the polycrystalline alloy and to about 4 Å in the spectra of the amorphous alloys (see Fig. 5). This corresponds to backscattering from neighbors five shells distant from the excited atom in the polycrystal and from only three shells in the amorphous alloys. Backscattering from boron atoms was excluded from the fits after testing different models. Adding this component never improved the fits or, in the best of the cases, its contribution was poor. Boron has many fewer electrons than Co or Fe and, therefore, its electron backscattering cross section is much smaller, making this one of the possible reasons that boron was apparently undetected in these spectra. The analysis of the amorphous alloys was carried out assuming atomic Gaussian distributions instead of asymmetric distributions. Asymmetric radial distribution functions have often been assumed for amorphous alloys of similar composition but produced by different methods other than sputtering deposition.[41,42,45] We tested asymetric distributions in our fits but the resulted asymmetry was negligible. The best fits to the EXAFS spectra were obtained for the polycrystalline alloys, using a structural model consisting of a mixture of two crystal phases, bcc and fcc, whereas for the amorphous alloys, a single phase with a short-range order similar to that of an fcc lattice was used. This model agrees with the expected bcc to fcc transition when boron (and cobalt) concentration is increased in the alloy.[22] The coexistence of bcc and fcc phases in this kind of alloys is not uncommon and it has been reported before.[22,23,46] The presence of highly disordered transition metal (TM)-metalloid (M) and TM-TM environments in the alloys should be added to this description. Despite the fact that a Gaussian atomic distribution produced the best fit for all the spectra, the atomic coordinations obtained from the fits were smaller than those expected (see Fig. 7). The highest difference was found in the amorphous alloys. A similar behavior has also been observed in other TM-M alloys, FeSi and CoSi, deposited by sputtering.[34] In those alloys, the TM-M environments were undetected by EXAFS for low M concentrations, and their presence evidenced only because the coordination of the TM-TM environments decreased. For large metalloid concentrations, only the TM-M environments were visible to EXAFS with unphysically small coordination, whereas the TM-TM environments apparently disappeared. The loss in coordination is explained assuming the presence of highly disordered atomic environments with an atomic distribution too wide to be detected by EXAFS. The relative concentration of these highly disordered atomic environments will scale with the difference between the coordination obtained from the fits and the expected one. For the amorphous alloys, this concentration was the highest and estimated to 60% in the most disordered case as can be calculated by comparing the expected values of coordination for a fcc lattice to those obtained (see Fig. 7).

The analysis of the spectrum of the polycristalline alloy included the same electron scattering paths than those used for the fit of the EXAFS spectrum of the Fe reference foil. These were all single scattering paths up to the 5th coordination shell and multiple scattering paths along the (111) and (100) directions. Important differences with respect to the fit of the Fe reference spectrum were observed, and interpreted as the presence of a second phase in the alloy based on the fcc phase of Fe. First, the first neighbors bond distance was appreciably larger [2.53(3) Å] than that in pure bcc Fe foil (2.49 Å). Second, the scattering path in the fourth shell [direction $\frac{1}{2}(113)$ in the bcc lattice] was not necessary and, instead, a single scattering path had to be included, indicating the presence of a third shell with an interatomic length of 3.6 Å. This distance is similar to

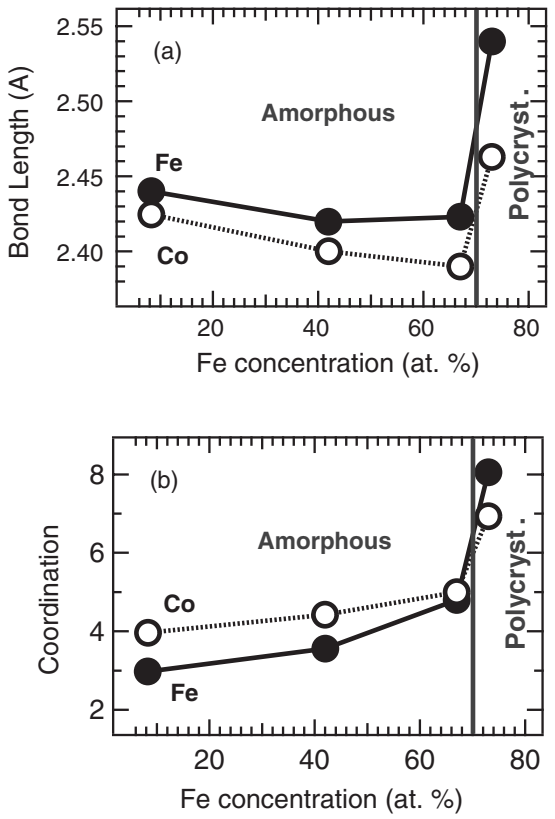

FIG. 7. (a) Bond length vs Fe concentration (atoms percent); (b) first neighbors coordination vs Fe concentration (Fe data, solid dots; Co data, empty dots). Coordination was obtained assuming a passive electron reduction factor S_0^2 of 0.75 for Fe and 0.9 for Co, deduced from the EXAFS spectra of polycrystaline Fe and Co foils. The polycrystalline alloy is the one with the highest Fe concentration.

the lattice parameter of an fcc lattice with a distance between first neighbors of 2.54 Å suggesting the presence of an fcc phase which is also found in the alloys with higher boron concentration.

To determine the proportion of bcc to fcc phases, we assumed that bcc environments were visible by EXAFS up to the fifth shell and fcc environments only up to the second shell. This was coherent with the comparison of the spectrum of polycrystalline FeCoB with the Fe standard (see Fig. 2). It also agrees with the result obtained in the samples with higher boron content. The coordination of the first shell, N_I, was expressed as a function of the relative concentration of bcc to fcc environments:

$$N_I = \gamma \left[N_I^{\mathrm{bcc}} \alpha + N_I^{\mathrm{fcc}} (1-\alpha) \right] \qquad (2)$$

where $N_I^{\mathrm{bcc}} = 8$ and $N_I^{\mathrm{fcc}} = 12$. Then, the coordination of the other shells was a function of its respective structural concentration [α for bcc and $(1-\alpha)$ for fcc environments] and the parameter γ. This parameter should be the passive electron reduction factor deduced from the spectra of the Fe and Co standards if only Fe and Co were present in the alloy. However, this parameter should be smaller in the FeCoB alloy because Fe and Co can also be coordinated to boron. The spectra were fitted using fixed values of γ. The best fit (smallest χ^2) determined its value. This procedure yields a concentration of bcc to fcc environments of about 50% with γ equal to 0.6 ($\pm$0.05) in Fe and 0.7 in Co. The value of γ is 10% smaller that the passive electron reduction factor obtained from the standards if boron is taken into account (the atomic concentration of boron was 10%). This loss in coordination might be caused by vacancies or by the presence of a largely disordered phase induced by boron, the same that seemed to cause the more important loss in coordination in the samples with 20% boron (see Fig. 7).

The fit of the spectrum of the amorphous alloys included single scattering paths up to the third shell assuming an fcc lattice, which was the one that better adjusted the data. However, the relationship between the radius of the different shells suggested a distortion in the fcc lattice. The radius of the first shell was 2.42 Å, significantly longer than that expected from the radius of the second (3.3 Å) and third (4.01 Å) shells that yield a first shell radius of 2.33 Å if atoms were arranged in an fcc lattice. This apparent distortion can be explained assuming more than a single environment in the alloy. It will be shown later on that the magnetostrictive phase detected by DiffEXAFS has a longer bond length (see Sec. IV A). Including this phase in the EXAFS spectra removes the apparent distortion of the fcc lattice that needs to be invoked if only one phase is included in the model. The resulting lattice parameter of the fcc cell after adding this phase is 3.44 Å. All the parameters used for the fits of the polycrystalline and amorphous alloys at the Fe K edge are summarized in Table I.

The EXAFS spectrum at the Co K edge was very similar in shape to that obtained at the Fe K edge, so the spectra were fitted in the same way. The parameters obtained from the best fits are shown in Table II. This table shows that all interatomic distances measured at the Co K edge are noticeably smaller. Figure 7 compares the first shell bond lengths measured at the two edges. Within the set of amorphous alloys, the largest difference (0.04 Å) is found for the sample with highest Fe concentration [$(Fe_{80}Co_{20})_{80}B_{20}$]. Since the shape of the spectra was the same, Co, which was minority in most of the analyzed alloys, should occupy similar positions in the lattice as Fe, acting as a substitutional impurity. The bond length reduction is the expected behavior, and is also observed in crystalline FeCo (whose lattice parameter is smaller than in bcc Fe for low Co concentrations).[47]

B. DiffEXAFS spectra

Figure 8 shows the raw DiffEXAFS spectra. At the Fe K edge, the amplitude of the DiffEXAFS spectrum decreases with Fe concentration and no signal is measured in the alloy with the lowest Fe concentration [$(Fe_{10}Co_{90})_{80}B_{20}$]. At the Co K edge, an appreciable signal is measured only in the alloy with the largest Co concentration. Only the spectra of the polycrystalline and amorphous alloys with the largest Fe and Co content, i.e., the samples $(Fe_{80}Co_{20})_{90}B_{10}$, $(Fe_{80}Co_{20})_{80}B_{20}$, and $(Fe_{10}Co_{90})_{80}B_{20}$ had sufficient S/N to be fitted. The spectrum of the alloy $(Fe_{50}Co_{50})_{80}B_{20}$ was corrupted at high energies (above 7.3 keV). The structure below this energy being very similar to that at higher Fe content, it was assumed that the relative data differed only by their amplitudes.

The DiffEXAFS spectrum is obtained by the difference between two EXAFS spectra, measured applying a magnetic

TABLE I. Parameters used for the fits of the EXAFS spectra of the FeCoB alloys $(Fe_{80}Co_{20})_{90}B_{10}$ (polycrystalline) and $(Fe_{80}Co_{20})_{80}B_{20}$ (amorphous) at the Fe K edge. The fits assumed that the polycrystal was the sum of a bcc phase (all shells except the third one in the table) and a fcc phase (only to second neighbors, first and third shells in the table), and the amorphous alloy was in a single phase with a fcc short-range order up to the third shell. A_E is the amplitude of the scattering path related to the specific shell without the correction of the passive electron reduction factor S_0^2, which was 0.75 in Fe, σ^2 is the width of the gaussian distribution, and R is the interatomic distance between the central atom and an atom in the specific shell. The number in brackets indicates the error in the last written decimal.

Shell	Polycrystal A_E	R	σ^2	Amorphous A_E	R	σ^2
1st	6.04(8) (bcc + fcc)	2.530(3)	0.0135(5)	3.6(2) (fcc)	2.42(5)	0.014(1)
2nd	2.9 (bcc)	2.872(3)	0.007(1)	1.8 (fcc)	3.32(2)	0.019(2)
3rd	3.1 (fcc)	3.59(1)	0.014(1)	7.2 (fcc)	4.01(2)	0.024(2)
4th	9 (bcc)	4.19(1)	0.05(1)	...	...	...
5th	6 (bcc)	5.02(1)	0.02(1)	...	...	...
6th	4.5 (bcc)	5.83(1)	0.02(1)	...	...	...

field $\vec{H}$ parallel and perpendicular to the x-ray polarization vector $\vec{E}$, respectively.[8] The equation that describes each electron scattering process in DiffEXAFS is obtained as the derivative of the EXAFS equation (1) with respect to R_i:[8,48]

$$\chi(k) = \sum_i \frac{2\delta R_i N_i S_0^2 f_i(k)}{R_i^2} e^{-2\sigma_i^2 k^2} e^{-2R_i/\lambda(k)} \cos[2kR_i + \phi_i(k)]. \quad (3)$$

Figure 9 displays the DiffEXAFS spectrum at the Fe K edge of the polycrystalline film after subtracting a background using the AUTOBAK function in IFEFFIT.[39] The representation of the spectrum in R space $[\chi(R)]$ shows almost the same features as its related EXAFS spectrum, both compared in Fig. 10. The most important difference between them is that the peaks related to scattering from external coordination shells are almost as intense as the first coordination shell. According to Eq. (3), this results from δR_i values that are larger for higher-order shells. The position of the peaks seems very similar in both spectra. To fit the data relative to the polycrystalline sample we used six shells, the same as in the EXAFS. The scattering paths are similar than those used to fit bcc Fe with two important differences: first, the second shell is split in two with very close distances (2.96 and 3.19 Å) and second, the lattice parameter is significantly larger (2.96 Å). Then, the magnetostrictive environment of Fe detected by DiffEXAFS seems to be a tetragonally distorted bcc lattice with a distortion ratio (c/a) of 1.08, and with a larger unit cell volume than bcc Fe. In addition, it differs from the average atomic environments determined by EXAFS.

The differences between the atomic environments detected by DiffEXAFS and EXAFS are better visualized in the case of the amorphous alloys. Figure 11 compares the DiffEXAFS and the EXAFS $\chi(R)$ spectra at the Fe K edge for $(Fe_{80}Co_{20})_{80}B_{20}$. The DiffEXAFS spectrum clearly shows that the magnetostrictive environments of the amorphous alloy have longer interatomic distances than those detected by EXAFS. The best fit is obtained using the first three shells used in the fit of the polycrystalline film (see Fig. 12). The amplitude of the second-neighbor shells (second and third paths in Table III) was largely reduced with respect to the polycrystal due to the larger disorder, but the interatomic distances were similar, indicating that the magnetostrictive environment found in the polycrystal was preserved to first neighbors in the amorphous state. The parameters used in the fits are shown in Table III.

Co magnetostriction environments were detected only in the alloy with highest Co concentration. Its DiffEXAFS spectrum is displayed in Fig. 13 and 14. The spectral shape was totally different to that observed at Fe and, more interestingly, the related magnetostriction coefficient was negative, i.e., the magnetostrictive lattice shrunk in the direction of the magnetic field instead of stretching as in Fe. This agrees with the strain observed in CoB amorphous alloys, which is negative.[5] The spectrum was well fitted using two coordination shells, at 2.49

TABLE II. Parameters used for the fits of the EXAFS spectra of the FeCoB alloys $(Fe_{80}Co_{20})_{90}B_{10}$ (polycrystalline) and $(Fe_{80}Co_{20})_{80}B_{20}$ (amorphous) at the Co K edge. The fits assumed that the polycrystal was the sum of a bcc phase (all shells except the third one in the table) and a fcc phase (only to second neighbors, first and third shells in the table), and the amorphous alloy was in a single phase with a fcc short-range order up to the third shell. A_E is the amplitude of the scattering path related to the specific shell without the correction of the passive electron reduction factor S_0^2, which was 0.9 in Co, σ^2 is the width of the Gaussian distribution, and R is the interatomic distance between the central atom and an atom in the specific shell. The number in brackets indicates the error in the last written decimal.

Shell	Polycrystal A_E	R	σ^2	Amorphous A_E	R	σ^2
1st	6.24(2) (bcc + fcc)	2.46(1)	0.012(1)	4.5(4) (fcc)	2.35(1)	0.011(1)
2nd	2.4 (bcc)	2.81(1)	0.004(1)	1.8 (fcc)	3.13(3)	0.016(3)
3rd	3.6 (fcc)	3.54(2)	0.022(2)	7.2 (fcc)	3.83(4)	0.037(6)
4th	9 (bcc)	4.02(2)	0.04(1)	...	...	...
5th	6 (bcc)	4.90(2)	0.02(1)	...	...	...
6th	4.5 (bcc)	5.65(5)	0.03(1)	...	...	...

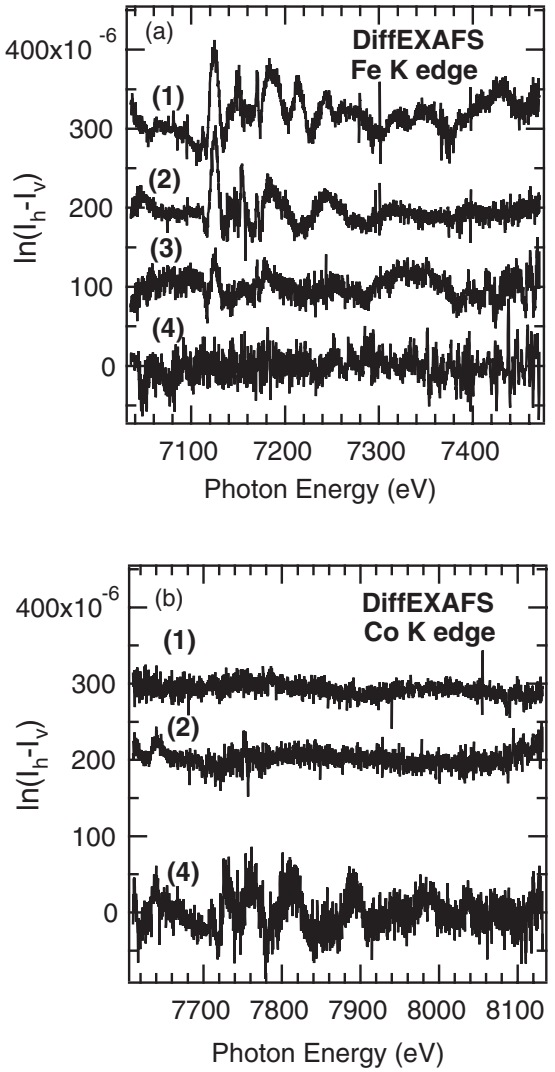

FIG. 8. DiffEXAFS spectra (raw data normalized to the incident beam intensity) of (1) $(Fe_{80}Co_{20})_{90}B_{10}$, (2) $(Fe_{80}Co_{20})_{80}B_{20}$, (3) $(Fe_{50}Co_{50})_{80}B_{20}$, and (4) $(Fe_{10}Co_{90})_{80}B_{20}$ at the Fe K edge (a) and the Co K edge (b). A constant background offset was added to each spectra to separate them.

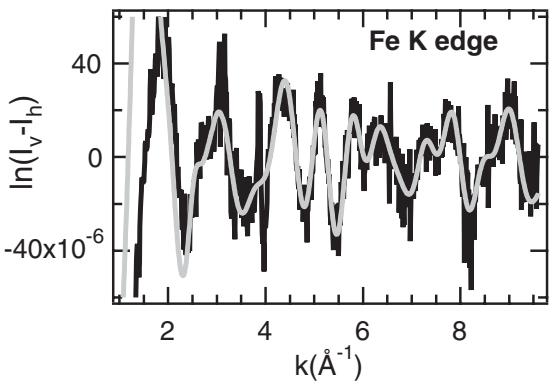

FIG. 9. DiffEXAFS spectrum of the polycristalline alloy $(Fe_{80}Co_{20})_{90}B_{10}$ at the Fe K edge. The fit of the spectrum (grey line) was done in between the k limits $k = 2.4$ Å^{-1} and $k = 9.5$ Å^{-1}.

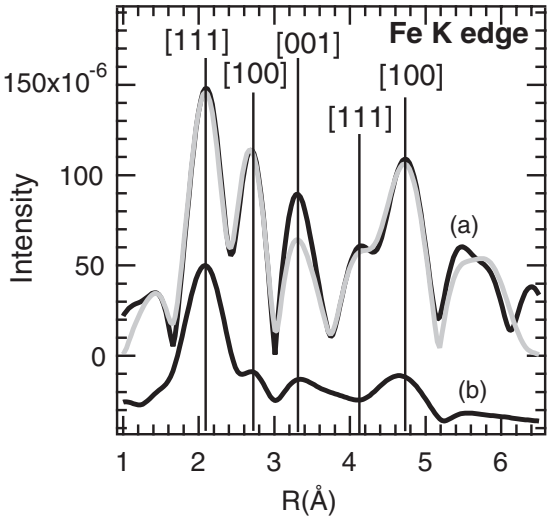

FIG. 10. (a) Fourier transform of the DiffEXAFS spectrum of the polycrystalline alloy $(Fe_{80}Co_{20})_{90}B_{10}$, compared to (b) its Fourier transformed EXAFS spectrum at the Fe K edge, which was reduced in amplitude for comparison. The fit of the DiffEXAFS spectrum is in gray. The brackets at the peaks of the DiffEXAFS spectrum indicate strain directions.

and 2.76 Å, respectively. As at the Fe K edge, the magnetostrictive environment of Co was completely different to the average environment detected by its related EXAFS (see Fig. 14).

The contribution from boron scattering also seemed to be negligible in the fits of the DiffEXAFS spectra. This could be caused by a TM-B strain too small to be detected, or due to similar reasons as those commented for the EXAFS spectra.

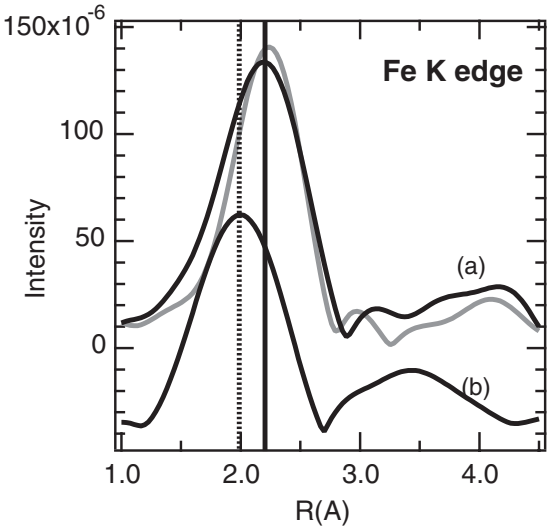

FIG. 11. (a) Fourier transform of the DiffEXAFS spectrum of the amorphous alloy $(Fe_{80}Co_{20})_{80}B_{20}$, compared to (b) its Fourier transformed EXAFS spectrum at the Fe K edge, which was reduced in amplitude for comparison. The fit of the DiffEXAFS spectrum is in grey.

TABLE III. Parameters used for the fits of the DiffEXAFS spectra of $(Fe_{80}Co_{20})_{90}B_{10}$ (polycrystalline) and $(Fe_{80}Co_{20})_{80}B_{20}$ (amorphous) at the Fe K edge. A_D is the amplitude of the scattering path related to the specific shell, σ^2 is the width of the Gaussian distribution, and R is the interatomic distance between the central atom and an atom in the specific shell. The number in brackets indicates the error in the last written decimal.

Shell	Polycrystal A_D	R	σ^2	Amorphous A_D	R	σ^2
1st	$3.9(3)\times10^{-2}$	2.68(1)	0.044(4)	$1.9(8)\times10^{-2}$	2.72(5)	0.02(3)
2nd	$0.6(3)\times10^{-2}$	2.96(1)	0.001(2)	$0.5(9)\times10^{-2}$	2.98(9)	0.006(9)
3rd	$0.5(5)\times10^{-2}$	3.19(1)	0.001(2)	$0.3(9)\times10^{-2}$	3.2(9)	0.003(9)
4th	$3.3(5)\times10^{-2}$	4.23(2)	0.04(1)	$3.5(1.5)\times10^{-2}$	4.5(7)	0.05(3)
5th	$8.1(5)\times10^{-2}$	5.13(2)	0.03(2)	...	...	...
6th	$1(5)\times10^{-2}$	5.97(2)	0.01(2)	...	...	...

IV. EXTRACTION OF ATOMIC MAGNETOSTRICTION COEFFICIENTS

In Secs. III A and III B, we have reported the analysis of the EXAFS and DiffEXAFS signals based on Eqs. (1) and (3), respectively. We have used standard EXAFS data analysis procedures and used for each a small number of scattering paths. We show that the EXAFS spectra for both the polycrystalline and amorphous samples can be described using relatively simple atomic models based on known crystal lattices (bcc and fcc) in a pure or mixed form. Here, the coordination numbers of the different shells have been constrained to the known shell progression. However, the models used to fit the DiffEXAFS spectra do not have this restriction because here [see Eq. (3)], the amplitude of the scattering path is proportional to the corresponding magnetostrictive atomic displacement for that path, i.e., it depends on the magnetostrictive coefficients of the alloy, which are unknown parameters.

Here, we describe a general method to extract the atomic magnetostriction coefficients from the combined EXAFS and DiffEXAFS data. In Secs. IV A and IV B, we apply this method, under different approximations, to the case of amorphous and polycrystalline FeCoB, respectively.

The EXAFS signal measured on our samples can be expressed as follows:

$$k\chi(k) = \sum_i A_{iE} \sin[2kR_i + \phi_i(k)], \tag{4}$$

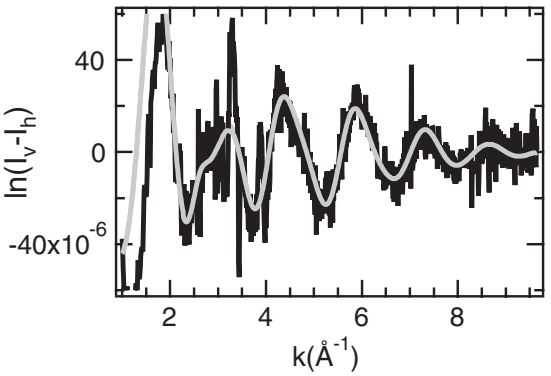

FIG. 12. DiffEXAFS spectrum of the amorphous alloy $(Fe_{80}Co_{20})_{80}B_{20}$ at the Fe K edge. The fit of the spectrum (grey line) was done in between the k limits $k = 2.4$ and 9.5 Å^{-1}.

where $A_{iE} = \frac{N_i S_0^2 f_i(k)}{R_i^2} e^{-2\sigma_i^2 k^2} e^{-2R_i/\lambda(k)}$ is the EXAFS amplitude of each path i [from Eq. (1)].

We can rewrite Eq. (4) as

$$\begin{aligned} k\chi(k) &= k\chi_{\mathrm{MS}}(k) + k\chi_{\mathrm{NMS}}(k) \\ &= \sum_i \{A_{iE_{\mathrm{MS}}} \sin[2kR_i + \phi_i(k)]\} \\ &\quad + \sum_j \{A_{iE_{\mathrm{NMS}}} \sin[2kR_j + \phi_j(k)]\}, \end{aligned} \tag{5}$$

where $k\chi_{\mathrm{MS}}(k)$ and $k\chi_{\mathrm{NMS}}(k)$ are the EXAFS contributions from the magnetostrictive (MS) and the nonmagnetostrictive (NMS) environments, respectively. The EXAFS analysis described in Sec. III A provides an average value of R_i and σ_i^2 over all environments (MS and NMS) and without further input it is impossible to separate the MS and NMS contributions.

The DiffEXAFS signal measured on our samples can be expressed as follows [from Eqs. (1), (3), and (4)]:

$$\begin{aligned} \chi(k) &= \sum_i A_{iD} \cos[2kR_i + \phi_i(k)] \\ &= \sum_i 2\delta R_i A_{iE_{\mathrm{MS}}} \cos[2kR_i + \phi_i(k)]. \end{aligned} \tag{6}$$

The DiffEXAFS analysis described in Sec. III B provides the structural parameters R_i and σ_i^2 for each path i in the magnetostrictive environments only. For each of these, we can define an atomic magnetostriction coefficient λ_{iD} measured by

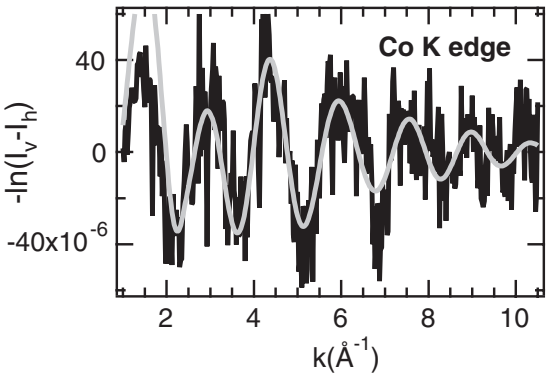

FIG. 13. DiffEXAFS spectrum of the Co-rich amorphous alloy $(Fe_{10}Co_{90})_{80}B_{20}$ at the Co K edge. It was multiplied by -1. The fit of the spectrum (grey line) was done in between the k limits $k = 2.4$ and 9.5 Å^{-1}.

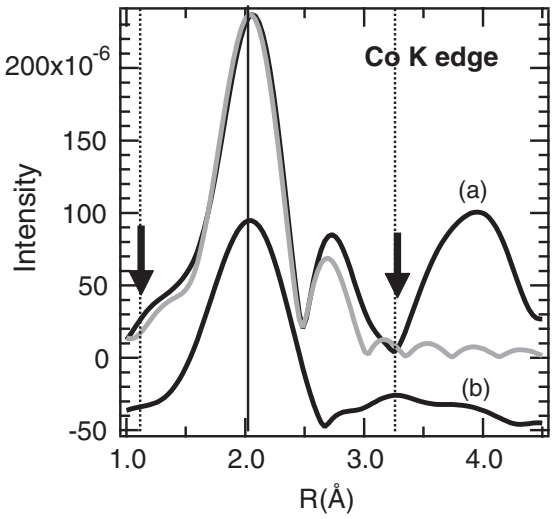

FIG. 14. Fourier transform of the DiffEXAFS spectrum of (a) the Co-rich amorphous alloy $(Fe_{10}Co_{90})_{80}B_{20}$, compared to (b) its Fourier transformed EXAFS spectrum, which was reduced in amplitude for comparison. The fit of the DiffEXAFS spectrum is in grey. The arrows indicate the limits in R space under which the spectrum was fitted.

DiffEXAFS as [from Eq. (6)]

$$\lambda_{iD} = \frac{\langle \delta R_i \rangle}{R_i} = A_{iD}/2R_i A_{iE_{\rm MS}}, \tag{7}$$

where $\langle \delta R_i \rangle$ is the strain averaged over all the orientations of the bond with respect to the magnetic field and the beam polarization vector, and $A_{iE_{\rm MS}}$ and A_{iD} are the amplitudes of EXAFS and DiffEXAFS that describe the electron scattering for that specific magnetostrictive environment using Eqs. (1) and (3), respectively. $\langle \delta R_i \rangle$ is related to the corresponding atomic magnetostriction coefficient λ_{iAt} by a proportionality factor K_i, i.e., $\lambda_{iD} = K_i \lambda_{iAt}$. This factor depends on the orientation of the magnetic field and the x-ray beam polarization vector with respect to the crystal axes. It is calculated in Appendix for an isotropic polycrystal with a cubic crystal lattice and for an isotropic amorphous material. There it is shown that K_i ranges from 3/2 for a perfectly oriented single crystal along the (111) or (100) orientations, to 0.675 in an isotropic polycrystal, or to 0.6 in an isotropic amorphous material.

In order to extract the λ_{iD} value for each magnetostrictive bond R_i and from these the microscopic (or atomic) magnetostriction coefficients λ_{iAt}, we need to evaluate $A_{iE_{\rm MS}}$ that appears in Eq. (6). To do this, we repeat the EXAFS analysis with all values of the structural parameters R_j and σ_j^2 of the magnetostrictive paths in Eq. (5) fixed to those obtained from the DiffEXAFS analysis [see Eq. (3)]. Free fitting parameters are the coordination numbers for the magnetostrictive paths and coordination numbers and structural parameters R_i and σ_i^2 of the nonmagnetostrictive paths. The reliability of this method depends strongly on the quality of the DiffEXAFS data. In general, the procedure works well for samples where the portion of magnetostrictive environments is relatively important.

In the case of the samples analyzed in this work, this analysis presented important error bars in the atom coordination due to the relatively large number of parameters to fit and the relatively small difference between the magnetostrictive and nonmagnetostrictive environments. Error bars were specially large in the case of the polycrystalline alloy $[(Fe_{80}Co_{20})_{90}B_{10}]$. For this reason, the procedure was applicable only for the case of the amorphous samples (see Sec. IV A below). In all cases where a precise evaluation of $A_{iE_{\rm MS}}$ from the data is not possible, EXAFS and DiffEXAFS data can be combined to obtain magnetostrictive coefficients comparable to those obtained through macroscopic measurements.

Notably for crystalline and polycrystalline samples, where a specific crystal direction can be associated to a specific EXAFS coordination shell, we can define a macroscopic magnetostriction coefficient λ_{iM} measured by DiffEXAFS as

$$\lambda_{iM} = \frac{\langle \delta R_i \rangle}{R_i} = A_{iD}/2R_i A_{iE}. \tag{8}$$

Note that here, contrary to Eq. (7), the total EXAFS amplitude of path i, A_{iE}, is used from Eq. (1). The corresponding magnetostriction coefficients $\lambda_i = \lambda_{iM}/K_i$ are comparable to macroscopic magnetostriction coefficients along the i crystalline direction.

Equation (8) is readily applicable, because the amplitudes A_{iD} and A_{iE} associated to a specific EXAFS coordination shell can be estimated directly from the DiffEXAFS and EXAFS R-space representation $[\chi(R)]$, which separates shells of different lengths. This is, of course, an approximation that can be applied only if the first coordinations shells [peaks in $\chi(R)$] are well differentiated. We have applied Eq. (8) to evaluate the macroscopic (average) magnetostriction coefficient in the case of the polycrystalline alloy (see Sec. IV B below).

A. Extraction of atomic magnetostriction coefficients in amorphous FeCoB

Figures 15 and 16 show the new fit of the EXAFS spectrum of the amorphous alloy $(Fe_{80}Co_{20})_{80}B_{20}$ following the procedure described in Sec. IV. To reduce error bars, only the coordination of the first shell of the magnetostrictive

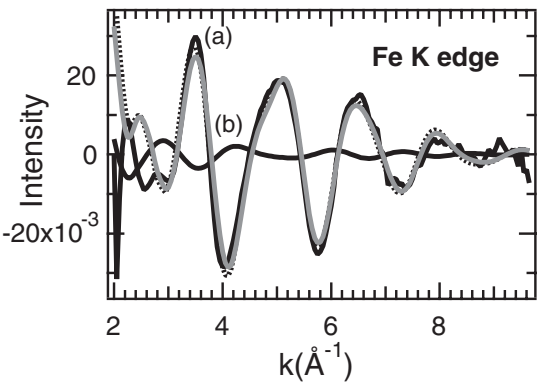

FIG. 15. (a) EXAFS spectrum of the amorphous alloy $(Fe_{80}Co_{20})_{80}B_{20}$ at the Fe K edge, fitted assumed two different atomic environments: one magnetostrictive, obtained from DiffEXAFS, and a nonmagnetostrictive environment. The spectrum marked as (b) is the resulting magnetostrictive component. The fit of the spectrum is a dotted line, whereas the spectrum attributed to the non-magnetostrictive phase is in grey. The fit was done in between the k limits $k = 2.9$ and 9.5 Å^{-1}.

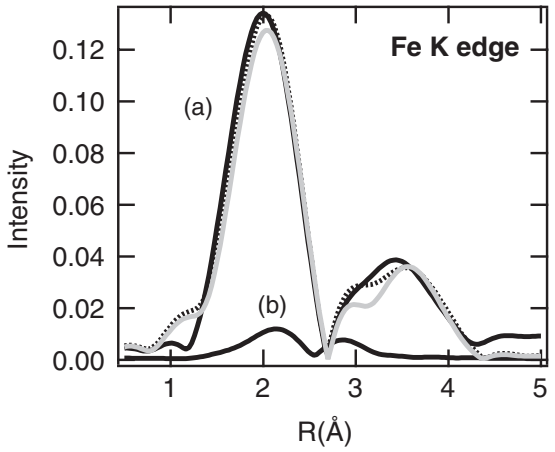

FIG. 16. (a) Fourier transform of the EXAFS spectrum of the amorphous alloy $(Fe_{80}Co_{20})_{80}B_{20}$ at the Fe K edge. The spectrum marked as (b) is the resulting magnetostrictive component. The fit of the spectrum is a dotted line, whereas the spectrum attributed to the nonmagnetostrictive phase is in grey.

environment was fitted, letting the others, corresponding to the second and third shells, to be proportional to it. The proportion of magnetostrictive phase $\frac{A_{E_{MS}}}{A_{E_{MS}}+A_{E_{NMS}}}$ obtained from this fit was 30±10%.

The fit assumed that the magnetostrictive phase was composed of small crystal units with a tetragonally distorted bcc lattice, as suggested by the values in Table III. The resulting magnetostriction cofficients for the Fe pairs were $\lambda_{111} = 181$ ppm and $\lambda_{100} = 160$ ppm.

Assuming that the strain was uniform in the sample (homogeneous and isotropic mechanical response of the nonmagnetostrictive regions and isotropic orientation of the magnetostrictive crystallites), the measured macroscopic magnetostriction coefficient λ_M for this alloy can be calculated from λ_{111} and λ_{100} by averaging the magnetostriction over all the possible orientations of each crystallite:[49]

$$\lambda_M = N_M \frac{2\lambda_{100} + 3\lambda_{111}}{5}, \quad (9)$$

where N_M is the fraction of atoms in the alloy that were magnetostrictive. This number was 30%(±10%) of the concentration of Fe atoms, yielding a macroscopic magnetostriction coefficient for this alloy of $\lambda_{Ma} = 34$ ppm, which is close to the value expected in these samples.[5–7] After the fitting, the nonmagnetostrictive phase was in a disordered fcc phase with a lattice parameter of 3.44 Å, correcting the previous mismatch between first and second neighbor interatomic distances observed when the magnetostrictive phase was not included in the fits. See Table IV with the parameters of the fit.

The fits for the polycrystalline sample including the magnetostrictive phase had error bars so large that results were unreliable. Whereas in the data relative to the amorphous alloy adding the magnetostrictive component helped to improve the fit, this was not the case for the data of the polycrystalline alloy, likely due to a lower concentration of the magnetostrictive component in this sample.

B. Macroscopic magnetostriction in polycrystalline FeCoB

By applying Eq. (8) and using $K_i = 0.65$ (in the assumption of an isotropic polycrystalline alloy)[see Eqs. (A9) and (A10) in Appendix], we obtain $\lambda_{111M} = 25$ ppm and $\lambda_{100M} = 46$ ppm. Averaging over all possible crystallite orientations using Eq. (9) (letting $N_M = 1$ since they are macroscopic magnetostriction coefficients) yields $\lambda_M = 33$ ppm, which is about 40% higher than that measured in this sample (20 ppm, see Fig. 2). Such a difference seems reasonable bearing in mind the approximations made to get the macroscopic coefficients starting from the DiffEXAFS data, where it was assumed that the mechanical response of the alloy to the strain of the magnetostrictive regions was uniform.[49] Such an assumption might not be applicable in these alloys whose heterogeneity has been demonstrated in this work. Note that if we apply the same procedure for the amorphous alloy $(Fe_{80}Co_{20})_{80}B_{20}$, the macroscopic magnetostriction coefficient obtained is $\lambda_M = 35$ ppm, which is almost the same as that deduced from the fits.

The related atomic magnetostriction coefficients in the polycrystalline alloy can be deduced if the concentration of its magnetostrictive phase in the alloy is known. We can speculate that the concentration of magnetostrictive environments is lower than in the amorphous sample, since the boron content is half that in the amorphous alloys. A lower concentration of magnetostrictive phase in the polycrystalline alloy is also expected since the highest magnetostriction is usually found on the fcc side of the phase diagram.[32] In fact, the magnetostriction coefficient of the polycrystalline alloy was lower (20 ppm) than the measured in the amorphous alloy (30 ppm) (see Fig. 2). If λ_{111} of the polycrystal was similar to the deduced from the fits in the amorphous alloy (about 180 ppm), the concentration of the magnetostrictive phase in

TABLE IV. Parameters used for the fits of the EXAFS spectrum of the amorphous alloy $(Fe_{80}Co_{20})_{80}B_{20}$ at the Fe K edge including the magnetostrictive components deduced from DiffEXAFS (fits shown in Fig. 15 and 16). A_{MS} and A_{NMS} are the amplitudes of the scattering paths related to the specific shell of the respectively magnetostrictive and nonmagnetostrictive components, σ^2 is the width of the gaussian distribution, and R is the interatomic distance between the central atom and an atom in the specific shell. The number in brackets indicates the error in the last written decimal.

Shell	A_{MS}	R	σ^2	A_{NMS}	R	σ^2
1st	1.9(6)	2.72(5)	0.02(3)	4.2(3)	2.46(1)	0.014(1)
2nd	0.5	2.98(9)	0.006(9)	2.08	3.44(5)	0.018(3)
3rd	0.3	3.2(9)	0.003(9)	8.32	4.12(5)	0.029(3)
4th	3.5	4.5(7)	0.05(3)	...	...	...

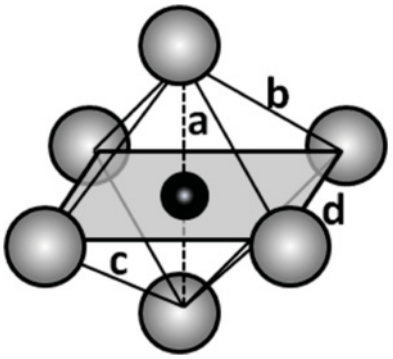

FIG. 17. Possible reconstruction of the magnetostrictive environment in the amorphous alloy. Fe are the grey spheres, and B is a black sphere. $a = 2.98$ Å (dashed line), $b = 2.72$ Å, and $c = d = 3.2$ Å.

the polycrystal would be 15%, and $\lambda_{100} = 300$ ppm. These values seem reasonable when compared with those found in FeCo ($\lambda_{111} = 70$ ppm and $\lambda_{100} = 270$ ppm) or with other iron-metalloid alloys like FeGa and FeAl ($\lambda_{100} = 400$ ppm).[12,13,16]

V. DISCUSSION

One of the most important findings of this experiment is that magnetostriction in FeCoB alloys originates only at specific atomic environments. The analysis of the polycrystalline alloy shows that these correspond to a tetragonally distorted bcc Fe lattice. In the amorphous state, the magnetostrictive atomic environment can be described with similar parameters, although second shells were significantly affected by disorder. The tetragonal lattice distortion in the polycrystalline alloy was likely caused by interstitial boron because the observed volume of the unit cell was larger than in bcc Fe. The present analysis cannot give the detailed position of the boron inside the cell but it probably occupies an octahedral site. This is also the preferred position for carbon and nitrogen interstitial impurities, which have a similar atomic radii than boron.[24–27] Actually, in the amorphous alloys, the Fe bond lengths found in the magnetostrictive environment are those expected if these Fe atoms were nearest neighbors of a boron impurity at an octahedral site. This is shown in Fig. 17. The observed distortion in the tetragonal structure has been theoretically predicted for carbon impurities instead of boron. In these calculations, the impurity modifies substantially the magnetic character of Fe, changing the sign of the exchange interaction (from negative to positive) and increasing its magnitude, making exchange the main driving force causing the impurity site distortion.[28] This is what seems to happen in the present case, i.e., the magnetostriction is localized at the impurity interstitial site. Actually this is what has been observed also in FeGa by DiffEXAFS, where the main contribution to the magnetostriction of the material came from the strain in the Fe-Ga bonds. The origin of the magnetostriction in this alloy is still under discussion. The models used to explain it can be taken as a reference to understand the magnetostriction in FeB since, as previously commented in the introduction, FeGa and FeB have several characteristics in common. In a first model, the magnetostriction is extrinsic: it is caused by the reorientation of specific tetragonal metastable defects to equivalent crystal directions by the effect of the magnetic field through direct spin-spin exchange interaction.[12,13] In the second model, the magnetostriction is intrinsic, i.e., it manifests itself because the strain dependence of the magnetocrystalline anisotropy strongly affects electron occupancy: the spin-orbit coupling changes critically with orbital occupancy, which at the same time is affected by the applied strain.[16] This model admits that magnetostriction should be stronger at the impurity site because it is where the $3d$ orbitals of Fe are more significantly modified with strain. In the extrinsic model, the magnetostriction coefficient λ_{111} along the diagonal direction should be identically zero since the (111) direction forms the same angle with respect to any of the tetragonal axis to where the crystallite (or magnetostrictive unit) can be reoriented. However, this coefficient is effectively large in both the polycrystalline and the amorphous alloys. Therefore the origin of the magnetostriction in FeB must be intrinsic but restricted to the specific interstitial impurity defects that tetragonally deform the site.

Another important point derived from this study is the role of Co in the magnetostrictive properties. For low Co concentrations, EXAFS showed that Co occupied substitutional positions in the Fe lattice. Magnetostriction derived from Fe-Co pairs was discarded in the polycrystalline alloy because the lattice parameter observed in its magnetostrictive environments was larger than that observed in polycrystalline FeCo.[8] Therefore, if Co had any participation in the magnetostriction of the polycrystalline alloy, it is as a substitutional impurity of Fe. In the amorphous state, with increasing Co concentration, the shape of the DiffEXAFS spectra at Fe is similar, indicating that Co does not have a significant effect in the magnetostrictive Fe environment. When Co is present at concentrations where it could cluster having Fe as a substitutional impurity, its magnetostrictive environment is completely different than that observed in the Fe rich alloys. The sign of the magnetostriction coefficient of magnetostrictive Co environments is negative indeed, explaining why magnetostrictive properties are reduced with increasing Co content.[5]

VI. CONCLUSIONS

DiffEXAFS served to identify the atomic environments responsible for the magnetostrictive properties of polycrystalline and amorphous FeCoB alloys. It proved that these alloys are heterogeneous: the magnetostrictive environments detected by DiffEXAFS are clearly different from the atomic environments detected by EXAFS. Magnetostriction is caused by the interaction between the transition metal, Fe or Co, with the metalloid boron, but only at specific sites. The analysis of the DiffEXAFS spectra in the polycrystalline and amorphous alloys indicates that the magnetostrictive environments of Fe are at tetragonally distorted octahedral interstitial sites occupied by boron impurities. Then, the positive magnetostriction observed in these alloys can be explained by the anisotropic change in volume caused by the rotation of the tetragonal axis of the octahedral site under an externally applied magnetic field. Magnetostriction from Fe-Co environments can be discarded even in the polycrystalline alloy. The detected magnetostrictive environment of Co differs from that found in Fe. Indeed, its related magnetostrictive coefficient is negative,

i.e., opposite to that of Fe, in agreement with the expected magnetostrictive behavior of the alloy with increasing Co concentration. The difficulties found in deconvolving the contribution of the magnetostrictive environments from their related EXAFS spectra demonstrates the extreme sensitivity of DiffEXAFS in detecting magnetostrictive environments. In the case of the polycrystalline alloy, this also suggests that the concentration of these environments is minor. Our analysis indicates that the corresponding magnetostrictive coefficients could be of similar magnitude than those found in other magntostrictive TM-M alloys like FeGa or FeAl.

ACKNOWLEDGMENTS

We are grateful for the skillfull assistance of the ID24 beamline technicians Sebastien Pasternak and Florian Perrin. Work supported by Spanish MICINN (Grant Nos. FIS2008-06249 and HP2008-0032).

APPENDIX: MAGNETOSTRICTION MEASURED BY DIFFEXAFS IN ISOTROPIC POLYCRYSTALS AND AMORPHOUS MATTER

This appendix shows how to deduce the proportionality factor K_i that relates the magnetostrictive coefficient λ_{iAt} associated to a specific atomic environment i, with the magnetostrictive coefficient λ_{iD} measured by DiffEXAFS in a disordered material:

$$\lambda_{iD} = K_i \lambda_{iAt}. \tag{A1}$$

The calculation will be done for an isotropic polycrystal with a cubic lattice and for an isotropic amorphous material.

To determine K_i, it is necessary to understand how the magnetostrictive solid deforms under the presence of magnetic fields and how DiffEXAFS measures the strains related to such a deformation. The main characteristic of DiffEXAFS is that it measures the strain between atoms whereas a macroscopic measurement of the strain in a solid measures its averaged deformation. One important consequence of this is that DiffEXAFS can give the magnetostriction coefficients of a crystal in a single measurement even if the studied sample is a polycrystal with randomly oriented crystallites, since it is able to distinguish the different atomic environments by their interatomic distance, specific coordination, and elemental composition. Coordination shells in EXAFS can be associated with crystal directions if atoms are located at the lattice sites, as is the case in Fe bcc or Co fcc. In a bcc crystal, the first coordination shell is related to the (111) direction, the second coordination shell to the (100) direction, and so on. Then, the variation in length of the ith coordination shells δR_i measured by DiffEXAFS is equivalent to the variations in length of the related crystal direction δR_{hkl}. The change in length for each crystal direction depends on the orientation of the crystal with respect to the applied magnetic field through its particular magnetostriction tensor. The magnetostriction coefficient λ_c of a cubic crystal describing its deformation from the demagnetized state to saturation can be calculated by the following expression:[50,51]

$$\lambda_c = \frac{3}{2}\lambda_{100}\left(\alpha_1^2\beta_1^2 + \alpha_2^2\beta_2^2 + \alpha_3^2\beta_3^2 - \frac{1}{3}\right) + 3\lambda_{111}\left(\alpha_1\alpha_2\beta_1\beta_2 + \alpha_2\alpha_3\beta_2\beta_3 + \alpha_1\alpha_3\beta_1\beta_3\right), \tag{A2}$$

where α_i and β_i are the cosines that define the saturation magnetization vector and the measurement direction, respectively, relative to the crystal axes. λ_{100} and λ_{111} are the magnetostriction coefficients for the related orientations in the cubic crystal. The saturated magnetostriction in the (111) direction in a cubic crystal when it changes from the demagnetized state to saturation with the magnetic field applied in the direction defined by the cosines α_i is

$$\lambda_{111}^{\phi,\theta} = \lambda_{111}\{\sin^2(\theta)\cos(\phi)\sin(\phi) + \cos(\theta)\sin(\theta)[\cos(\phi) + \sin(\phi)]\}, \tag{A3}$$

where $\vec{\beta} = \frac{1}{\sqrt{3}}(111)$ and $\vec{\alpha} = [\sin(\theta)\cos(\phi), \sin(\theta)\sin(\phi), \cos(\theta)]$ in spherical coordinates.

DiffEXAFS measures the difference in strain for a certain atomic bond in a crystal between two orientations of the magnetic field that are orthogonal to each other. The cosines that define the direction of the orthogonally oriented magnetic field will be $\vec{\alpha_\perp} = [\cos(\theta)\cos(\phi), \cos(\theta)\sin(\phi), -\sin(\theta)]$. Then, the strain measured by DiffEXAFS in the (111) direction in a crystallite at any orientation with respect to the magnetic field will be the difference between the strain deduced in Eq. (A3) and that obtained using Eq. (A2) with the orientation of the magnetic field given by $\vec{\alpha_\perp}$:

$$\delta R_{111}^{\phi,\theta} = R_{111}\,\lambda_{111}^{\phi,\theta} = R_{111}\,\lambda_{111}\{\sin(2\theta)[\cos(\phi) + \sin(\phi)] - \cos(2\theta)\cos(\phi)\sin(\phi)\}. \tag{A4}$$

Using a similar reasoning, the measured strain in the 100 direction will be

$$\delta R_{100}^{\phi,\theta} = R_{100}\,\lambda_{100}^{\phi,\theta} = R_{100}\,\frac{3}{2}\lambda_{100}[\sin^2(\theta) - \cos^2(\theta)]\cos^2(\phi). \tag{A5}$$

The polarization dependence of DiffEXAFS is $3\cos^2(\theta_i)$, θ_i being the angle between the measured direction and the polarization $\vec{E}$ of the beam.[43] Since $\vec{E}$ is parallel to $\vec{\alpha}$, $3\cos^2(\theta_i) = 3\langle\vec{\alpha},\vec{\beta_i}\rangle^2$. If $\vec{\beta_i}$ is the (100) direction, then

$$3\cos^2(\theta_i) = 3\sin^2(\theta)\cos^2(\phi). \tag{A6}$$

For the (111) direction,

$$3\cos^2(\theta_i) = \{1 + \sin^2(\theta)\sin(2\phi) + \sin(2\theta)[\cos(\phi) + \sin(\phi)]\}. \tag{A7}$$

If the sample is an untextured polycrystal, the measured δR_i will be averaged over all the possible crystallite orientations weighted by their orientation relative to the beam polarization $\vec{E}$:

$$\langle\delta R_i\rangle = \frac{1}{4\pi}\int_{\theta=0}^{\pi}\int_{\phi=0}^{2\pi} 3\cos^2(\theta_i)\delta R_i^{\phi,\theta}\sin(\theta)d\theta d\phi. \tag{A8}$$

When this integral is done for the (111) and (100) directions, the result is

$$\langle \delta R_{111} \rangle = \frac{2}{3} \lambda_{111} R_{111} \tag{A9}$$

and

$$\langle \delta R_{100} \rangle = 0.675\, \lambda_{100} R_{100}. \tag{A10}$$

The treatment of the magnetostriction in an amorphous material is a bit different than in an isotropic polycrystalline. DiffEXAFS measures the magnetostrictive strain of a specific crystal direction averaged over all the possible orientations of the crystal with respect to the fixed magnetic direction. That is why, in the above calculations, the β_i cosines were fixed to the specific crystal orientation whereas the α_i cosines, related to the orientation of the magnetic field with respect to the crystallite, were varied. In an amorphous material, EXAFS has usually access to first neighbors only. This means that there is only a single magnetostriction coefficient, which is related to the bond length strain. In this case, the β_i cosines, which represent the bond orientation, will be varied with respect to the α_i cosines which will be fixed. The magnetostriction coefficient of a material with a single strain axis can be deduced from that of a cubic structure [see Eq. (A2)] assuming that λ_{111} and λ_{100} are equivalent, i.e., they can not be distinguished:

$$\langle \lambda_M \rangle = \frac{3}{2} \lambda_a \left[(\alpha_1\beta_1 + \alpha_2\beta_2 + \alpha_3\beta_3)^2 - \frac{1}{3} \right]. \tag{A11}$$

Then, if the cosines of the magnetic field are taken along the axis directions (100) and (010), the strain δR_a in the atomic environment at a certain atomic pair orientation $\vec{\beta}_i$ measured by DiffEXAFS will be

$$\langle \delta R_a \rangle = \frac{3}{2} R_a \lambda_a [\sin^2(\theta)\cos^2(\phi) - \sin^2(\theta)\sin^2(\phi)]. \tag{A12}$$

When the average is carried out over all possible orientations of the strained bond respect to the x-ray beam polarization direction, the result is a bit smaller than that obtained for an isotropic polycrystal:

$$\langle \delta R_a \rangle = 0.6\, \lambda_a R_a. \tag{A13}$$

Therefore the proportionality factor K_i between the measured λ_{iD} and the microscopic λ_{iAt} will range from 3/2 for a perfectly oriented single crystal, to 0.666 if measuring λ_{100} in an isotropic polycrystal (0.675 when measuring λ_{111}), or to 0.6 in an isotropic amorphous material.

*jidiaz@uniovi.es

[1] H. W. Sheng, W. K. Luo, F. M. Alamgir, J. M. Bai, and E. Ma, Nature (London) **439**, 419 (2006).
[2] A. Evteev, A. Kosilov, and E. Levtchenko, Acta Mater. **51**, 2665 (2003).
[3] M. R. J. Gibbs, J. Magn. Magn. Mater. **83**, 329 (1990).
[4] E. R. Callen and H. B. Callen, Phys. Rev. A**139**, 455 (1965).
[5] R. C. O'Handley, Phys. Rev. B **18**, 930 (1978).
[6] R. C. O'Handley, M. C. Narasimhan, and M. O. Sullivan, J. Appl. Phys. **50**, 1633 (1979).
[7] K. Narita, J. Yamasaki, and H. Fukunaga, J. Appl. Phys. **50**, 7591 (1979).
[8] R. F. Pettifer, O. Mathon, S. Pascarelli, M. D. Cooke, and M. R. J. Gibbs, Nature (London) **435**, 78 (2005).
[9] J. Goldman and R. Smoluchowski, Phys. Rev. **75**, 140 (1949).
[10] J. R. Cullen, A. E. Clark, M. Wun-Fogle, J. B. Restor, and T. A. Lograsso, J. Magn. Magn. Mater. **948**, 226 (2001).
[11] M. Wuttig, L. Dai, and J. Cullen, Appl. Phys. Lett. **80**, 1135 (2002).
[12] A. G. Khachaturyan and D. Viehland, Metall. Mater. Trans. A **38**, 2308 (2007).
[13] A. G. Khachaturyan and D. Viehland, Metall. Mater. Trans. A **38**, 2317 (2007).
[14] S. Bhattacharyya, J. R. Jinschek, A. Khachaturyan, H. Cao, J. F. Li, and D. Viehland, Phys. Rev. B **77**, 104107 (2008).
[15] H. Cao, P. M. Gehring, C. P. Devreugd, J. A. Rodriguez-Rivera, J. Li, and D. Viehland, Phys. Rev. Lett. **102**, 127201 (2009).
[16] Y. N. Zhang, J. X. Cao, and R. Q. Wua, Appl. Phys. Lett. **96**, 062508 (2010).
[17] M. P. Ruffoni, S. Pascarelli, R. Grössinger, R. S. Turtelli, C. Bormio-Nunes, and R. F. Pettifer, Phys. Rev. Lett. **101**, 147202 (2008).
[18] E. M. Summers, T. A. Lograsso, and M. Wun-Fogle, J. Mater. Sci. **42**, 9582 (2007).
[19] J. I. Budnick, F. H. Sanchez, Y. D. Zhang, M. Choi, W. A. Hines, Z. Y. Zhang, S. H. Ge, and R. Hasegawa, IEEE Trans. Magn. **MAG-23**, 1937 (1987).
[20] I. G. Wood, L. VocÏadlo, K. S. Knight, D. P. Dobson, W. G. Marshall, G. D. Pricea, and J. Brodholta, J. Appl. Crystallogr. **37**, 82 (2004).
[21] E. Duman, M. Acet, E. F. Wassermann, J. P. Itié, F. Baudelet, O. Mathon, and S. Pascarelli, Phys. Rev. Lett. **94**, 075502 (2005).
[22] M. W. Ruckman, R. A. Levy, A. Kessler, and R. Hasegawa, J. Non-Cryst. Solids **40**, 393 (1980).
[23] H. Hermann and N. Mattern, J. Phys. F **16**, 131 (1986).
[24] Y. Hirotsu, R. Akada, and A. Onishi, J. Non-Cryst. Solids **74**, 97 (1985).
[25] K. Mitsukoa, H. Miyajima, H. Ino, and S. Chikazumi, J. Phys. Soc. Jpn. **53**, 2381 (1984).
[26] S. Y. Hong and A. B. Anderson, Phys. Rev. B **40**, 7508 (1989).
[27] C. Domain, C. S. Becquart, and J. Foct, Phys. Rev. B **69**, 144112 (2004).
[28] D. W. Boukhvalov, Y. N. Gornostyrev, M. I. Katsnelson, and A. I. Lichtenstein, Phys. Rev. Lett. **99**, 247205 (2007).
[29] N. Ito, K. Suzuki, J. S. Garitaonandia, and J. D. Cashion, J. Appl. Phys. **105**, 07A321 (2009).
[30] Q. Xing, T. A. Lograsso, M. P. Ruffoni, C. Azimonte, S. Pascarelli, and D. J. Miller, Appl. Phys. Lett. **97**, 072508 (2010).
[31] S. Pascarelli, M. P. Ruffoni, A. Trapananti, O. Mathon, C. Detlefs, M. Pasquale, A. Magni, C. P. Sasso, F. Celegato, E. Olivetti, Y. Joly, and D. Givord, Phys. Rev. B **81**, 020406R (2010).
[32] Y. Nakamura., IEEE Trans. Magn. **MAG-12**, 278 (1976).
[33] T. I. Hiroshi Tomita and T. Mizoguchi, IEEE Trans. Magn. **32**, 4529 (1996).
[34] J. Díaz, R. Morales, S. M. Valvidares, and J. M. Alameda, Phys. Rev. B **72**, 144413 (2005).

[35]A. C. Tam, and H. Schroeder, IEEE Trans. Magn. **25**, 2629 (1989).
[36]D. Ciudad, I.Lucas, C.Aroca, J. L. Prieto, and P. Sánchez, J. Appl. Phys. **101**, 043907 (2007).
[37]F. E. Luborsky, *Amorphous Metallic Alloys* (Butterworths, London, 1983).
[38]S. Pascarelli, O. Mathon, M. Muñoz, T. Mairs, and J. Susini, J. Synchrotron Radiat. **13**, 351 (2006).
[39]M. Newville, J. Synchrotron Radiat. **8**, 322 (2001).
[40]A. Yang, H. Imrane, J. Lou, J. Kirkland, C. Vittoria, N. Sun, and V. G. Harris., J. Appl. Phys. **103**, 07E736 (2008).
[41]M. L. Fdez-Gubieda, I. Orúe, F. Plazaola, and J. M. Barandiarán, Phys. Rev. B **53**, 620 (1996).
[42]M. L. Fdez-Gubieda, A. García-Arribas, J. M. Barandiarán, R. L. Antón, I. Orue, P. Gorria, S. Pizzini, and A. Fontaine, Phys. Rev. B **62**, 5746 (2000).
[43]E. A. Stern, *X-Ray Absorption: Principles, Applications, Techniques of EXAFS, SEXAFS and XANES,* edited by D. C. Koningsberger and R. Prins (Wiley, New York, 1988), pp. 3–51.
[44]J. J. Rehr and R. C. Albers, Phys. Rev. B **41**, 8139 (1990).
[45]E. D. Crozier, J. J. Rehr, and R. Ingalls, *X-Ray Absorption: Principles, Applications, Techniques of EXAFS, SEXAFS and XANES,* edited by D. C. Koningsberger and R. Prins (Wiley, New York, 1988), pp. 385–442.
[46]R. Hasegawa and R. Ray, J. Appl. Phys. **49**, 4174 (1978).
[47]G. A. Prinz, Phys. Rev. Lett. **54**, 1051 (1985).
[48]M. P. Ruffoni, J. Synchrotron Radiat. **16**, 591 (2009).
[49]B. D. Cullity, *Introduction to Magnetic Materials* (Addison-Wesley, Reading, Massachusetts, 1972), pp. 262–263.
[50]C. Kittel, Rev. Mod. Phys. **21**, 541 (1949).
[51]E. W. Lee, Rep. Prog. Phys. **18**, 184 (1955).